Honeywell

DARPA ZENITH PHASE-I

FERROHYDRODYNAMIC M&S SOFTWARE

Prime Organization	Honeywell Aerospace Technologies
Authors	Á. Romero-Calvo, H. Chen, T. Hu, E. Comstock, G. Cano-G´omez, M. Herrada
Author's Organization	Low-Gravity Science and Technology Laboratory Georgia Institute of Technology
Report Release	Technical Report LGST-2024-001 (Version 2) Public Release
Date	June 27, 2024
Abstract	This technical report summarizes the preliminary ferrohydroynamic analysis codes developed as part of Phase I of the DARPA Zenith Program (HR0011366236) under contract with Honeywell Aerospace Technologies (FA237724CB011).

Technical Report

LGST-2024-001 (Version 2)

Public Release

DARPA ZENITH PHASE-I FERROHYDRODYNAMIC M&S SOFTWARE

Á. Romero-Calvo, H. Chen, T. Hu, E. Comstock, G. Cano-Gómez, M. Herrada

Low-Gravity Science and Technology Laboratory

Georgia Institute of Technology

June 27, 2024

Abstract: This technical report summarizes the preliminary ferrohydroynamic analysis codes developed as part of Phase I of the DARPA Zenith Program (HR0011366236) under contract with Honeywell International Inc. (FA237724CB011).

Contents

Version	Date	Changed Chapters	Remarks
1	06/28/2024	4-6	Final Version
0	04/05/2024	All	First Version

Team Members

Álvaro Romero-Calvo, PhD
Position: Assistant Professor, Daniel Guggenheim School of Aerospace Engineering, Georgia Institute of Technology
Role: Georgia Tech Principal Investigator
email: alvaro.romerocalvo@gatech.edu

Hugh Chen
Position: Graduate Research Assistant, Daniel Guggenheim School of Aerospace Engineering, Georgia Institute of Technology
Role: Modeling & Simulation

Tianyang Hu
Position: Graduate Research Assistant, Daniel Guggenheim School of Aerospace Engineering, Georgia Institute of Technology
Role: Modeling & Simulation

Eric Comstock
Position: Graduate Research Assistant, Daniel Guggenheim School of Aerospace Engineering, Georgia Institute of Technology
Role: Modeling & Simulation

Gabriel Cano-Gómez, PhD
Position: Professor, Applied Physics III Department, Higher Technical Engineering School, University of Seville
Role: Ferrohydrodynamics support

Miguel Herrada, PhD
Position: Professor, Applied Physics III Department, Higher Technical Engineering School, University of Seville
Role: Capillary fluid mechanics support

Nomenclature

α	Tilting angle	rad
$\boldsymbol{B}$	Magnetic flux density	T
b	Magnet depth	m
β	Ratio of fifth-order to first-order effects	1
χ_0	Initial magnetic susceptibility of the ferrofluid	1
χ	Magnetic susceptibility	1
Δn	Increment in nanoparticle density	m^{-3}
δ	Ferrofluid thickness	m
ϵ	Ferrofluid surface wave amplitude	m
κ	Heuristic nanoparticle concentration parameter	
f	Mass-specific body force	$\mathrm{N\,m^{-3}}$
$F_{1,2}$	Heuristic fluid oscillation wave parameter	
$\boldsymbol{f}_m^V$	Kelvin body force	$\mathrm{N\,m^{-3}}$
$\boldsymbol{g}$	Gravitational acceleration	$\mathrm{m\,s^{-2}}$
Γ	Intermediate fluid surface oscillation parameter	
γ	Ferrofluid property	$\mathrm{m\,A^{-1}}$
$\boldsymbol{H}_0$	External magnetic field	$\mathrm{A\,m^{-1}}$
$\boldsymbol{H}$	Magnetic field	$\mathrm{A\,m^{-1}}$
h	Distance from ferrofluid layer to the top surface of the Halbach array	m
$\boldsymbol{H}_d$	Demagnetization field	$\mathrm{A\,m^{-1}}$
$\boldsymbol{H}_H$	Halbach magnetic field	$\mathrm{A\,m^{-1}}$
H_{01}	First-order magnetic field	$\mathrm{A\,m^{-1}}$
H_x	Magnetic field tangent to the ferrofluid surface	$\mathrm{A\,m^{-1}}$
k	Magnetic wave number	$\mathrm{m^{-1}}$
κ	Surface curvature	$\mathrm{m^{-1}}$
K	Equivalent magnetization current	$\mathrm{A\,m^{-1}}$
λ	Magnetic wavelength	m
L_x	Langevin function	1
$\boldsymbol{M}_0$	Magnet magnetization	$\mathrm{A\,m^{-1}}$
$\boldsymbol{M}$	Magnetization	$\mathrm{A\,m^{-1}}$
M_s	Ferrofluid saturation magnetization	$\mathrm{A\,m^{-1}}$
M_c	Critical magnetization	$\mathrm{A\,m^{-1}}$
M_n	Normal magnetization	$\mathrm{A\,m^{-1}}$
$\boldsymbol{p}_m^S$	Magnetic normal traction	m
μ_0	Vacuum permeability	$\mathrm{H\,m^{-1}}$
μ_c	Chord permeability	$\mathrm{H\,m^{-1}}$
μ_t	Tangent permeability	$\mathrm{H\,m^{-1}}$
n_0	Average nanoparticle density	$\mathrm{m^{-3}}$
M_0	Layer magnetization	$\mathrm{m^{-1}}$

ϕ	Volumetric magnetic particle concentration of the ferrofluid	1
Π	Mass-specific potential energy	$\mathrm{kg}^2\,\mathrm{m}^{-2}$
Π_g	Gravitational mass-specific potential energy	$\mathrm{kg}^2\,\mathrm{m}^{-2}$
Π_m	Magnetic mass-specific potential energy	$\mathrm{kg}^2\,\mathrm{m}^{-2}$
p^*	Composite pressure	Pa
p_0	Gas pressure	Pa
Φ^H	Magnetic scalar potential	A
p_m	Magnetic pressure	Pa
ρ	Ferrofluid density	$\mathrm{kg}\,\mathrm{m}^{-3}$
r_0	Geometric mean of chord and tangent permeabilities	1
σ	Surface tension	$\mathrm{N}\,\mathrm{m}^{-1}$
θ	Halbach array tilting angle	rad
$\boldsymbol{u}$	Reference system	1
w	Magnet width	m
ξ	Ratio of ferrofluid saturation magnetization to magnetic field strength	1
x	Horizontal position	m
y	Vertical position	m

1 Overview

1.1 DARPA Zenith Program

The DARPA Zenith program investigates liquid-mirror technology as an alternative to glass or beryllium optics. **Liquid-mirror telescopes (LMTs)** operate on the physics principle that the surface of a fluid can form a paraboloid (3D-dish shape) that is ideal for focusing light. The advantages of liquid mirrors over glass include easier and lower cost of fabrication, theoretical-max resolution (diffraction-limited), resilience to damage and potential ability to self-repair, elimination of regular costly mirror recoating and weather-protective domes, and scalability to much larger optics sizes.

LMTs have existed for many years, but significant limitations have hindered their utility. The biggest drawback is that ground-based LMTs are zenith-restricted, meaning they can only look straight up. Tilting the telescope at an angle causes the paraboloid to lose shape and the liquid to spill out of the baseplate. The delicate force balance needed to mathematically guarantee a light-focusing shape requires the rotation axis to be exactly vertical. For space-based LMTs, the need for spacecraft thrust to induce gravity requires the use of limited fuel resources, and rotation of the spacecraft to form the parabolic imaging surface creates increased design complexity.

In the context of the DARPA Zenith Program, the Low-Gravity Science and Technology Lab at the Georgia Institute of Technology has worked with Honeywell Aerospace and Soter Technology to design and demonstrate a self-assembling liquid mirror telescope with off-axis tilting and slewing capabilities. The effort explores the use of **Halbach arrays**, a particular arrangement of permanent magnets that produces one-sided magnetic fields [1], to manipulate ferrofluids to the desired optical shape. Ferrofluids are colloidal suspensions of magnetic nanoparticles in a carrier liquid [2]. The Halbach array (and the Mallinson magnetic configuration from which it derives [3]) generates equipotential lines that become quasi-parallel to its surface [4], overcoming the force of gravity for a ground-based liquid mirror telescope through the adjustment of internal magnetic configurations. The ferrofluid, in combination with immiscible ionic liquids containing reflective nanoparticles, is forced to create a liquid mirror surface with the desired optical shape, all while maintaining an acceptable wavefront error. Such innovation has potential for both terrestrial and orbital deployment, alongside the advantage of off-axis observation in contrast to traditional liquid mirror telescopes.

This technical report describes the tools developed for the modeling, simulation, and optimization of the magnetic Halbach array system. Section 1.2 provides a brief overview of the key theoretical aspects of the problem, while Sec. 1.3 lists the codes included in the report. Sections 2-7 expand on the assumptions, structure, and I/O operations of each code.

1.2 Theoretical Background

1.2.1 Ferrohydrostatics

The equilibrium state of a ferrofluid subject to static magnetic fields is driven by the Kelvin body force

$$\boldsymbol{f}_m^V = \mu_0(\boldsymbol{M}\cdot\nabla)\boldsymbol{H} = \mu_0 M\nabla H, \tag{1}$$

where μ_0 is the permeability of free space, $\boldsymbol{H}$ is the magnetic field, and $\boldsymbol{M}$ is the magnetization field, and the magnetic normal traction at the liquid interface

$$\boldsymbol{p}_m^S = \frac{\mu_0}{2}\,[M_n^2]\boldsymbol{n}, \tag{2}$$

with M_n being the normal component of the magnetization field with respect to the liquid surface [5]. In equilibrium, the momentum conservation equation reduces to the Euler condition [6]

$$\rho\left(\boldsymbol{g}+\frac{\mu_0}{\rho}M\nabla H\right)+\nabla p^*=\mathbf{0}, \tag{3}$$

where p^* denotes the composite pressure term [2]. In addition, the liquid interface is subject to the normal fluid-magnetic balance

$$p^*+p_m-p_0=2\sigma\kappa, \tag{4}$$

where p_0 is the pressure of the gas in contact with the interface, σ the surface tension of the liquid, and κ the mean curvature of the interface. The magnetic terms in these expressions are computed from the magnetostatic Maxwell equations which, in the problems under consideration, are also free from electric currents, resulting in [7]

$$\nabla\cdot\boldsymbol{B}=0, \tag{5a}$$

$$\nabla\times\boldsymbol{H}=\mathbf{0}, \tag{5b}$$

with $\boldsymbol{B}=\mu_0(\boldsymbol{H}+\boldsymbol{M})$ being the magnetic flux density field. The magnetic boundary conditions are

$$\boldsymbol{n}\cdot[\boldsymbol{B}]=0, \tag{6a}$$

$$\boldsymbol{n}\times[\boldsymbol{H}]=\mathbf{0}, \tag{6b}$$

where [-] denotes the difference across the interface. A constitutive relation of the form

$$\boldsymbol{M}=\chi(H)\boldsymbol{H} \tag{7}$$

is assumed in the ferrofluid, with $\chi(H)$ being its magnetic susceptibility and $\boldsymbol{H}$ the *internal* magnetic field inside the ferrofluid; that is, the superposition of the external $\boldsymbol{H}_0$ created by the magnetic devices and the demagnetization field $\boldsymbol{H}_d$ due to the polarization of the ferrofluid. An implicit assumption of Eq. 7 is that magnetization and magnetic fields are collinear.

A rigorous approach to the ferrohydrostatic problem requires solving the Euler condition in Eq. 3 together with the Maxwell equations in Eq. 5 with their corresponding boundary conditions, as the position of the ferrofluid determines the magnetic field, and the magnetic field, the position. However, for low-density ferrofluids like those considered in this work, the computation of $\boldsymbol{H}_d$ can be simplified or neglected, effectively decoupling the problem and simplifying the analysis [5]. By further considering an isothermal ferrofluid medium [8], the mass-force potential of the gravity and Kelvin body forces becomes

$$\Pi=gz-\frac{\mu_0}{\rho}\int_0^H M(H)dH, \tag{8}$$

and the Euler condition in Eq. 3 reduces to

$$p^*=-\rho\Pi+c', \tag{9}$$

with c' denoting an integration constant. After inserting this expression in the normal fluid-magnetic surface balance, the result is

$$\rho\Pi-p_m=-2\sigma\kappa+c, \tag{10}$$

where c is the modified integration constant. Equation 10 defines the equilibrium position of an isothermal ferrofluid interface subject to magnetic, capillary, and gravitational forces. However, it can be further simplified by assuming (i) low-density ferrofluids with initial magnetic susceptibilities $\chi\ll 1$ for

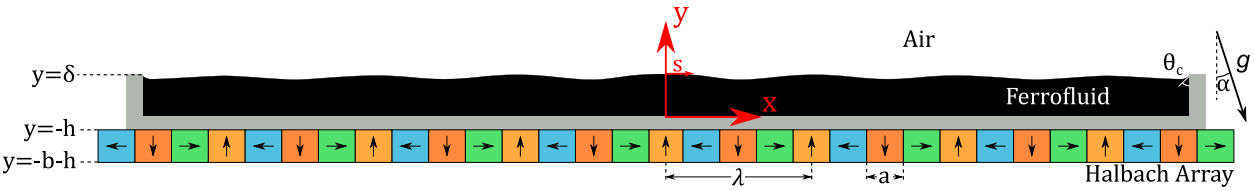

Fig. 1: Conceptual Halbach array representation

which $p_m \approx 0$, and (ii) inertia/magnetic-dominated regimes for which the Bond and magnetic Bond numbers are much greater than 1 and, therefore, $2\sigma\kappa \ll \Delta\Pi$. Under these assumptions,

$$\Pi \approx c', \tag{11}$$

or, in other words, the ferrofluid interface follows the constant equipotential line.

The different programs included in this report switch between different levels of physical accuracy depending on the scope of the code. When the global deformation of the ferrofluid interface subject to gravitational tilt is of interest, the equipotential theory is adopted as the baseline for the analysis. If the micrometer-level deformations induced by the Halbach array on the ferrofluid interface are to be analyzed, then Eq. 10 is solved under reasonable approximations of the demagnetization field and surface tension forces. To speed up the development of the technology and facilitate the exploration of the design trade space, a decoupling is imposed between (i) large-scale and (ii) small-scale deformations of the ferrofluid interface.

1.2.2 The Halbach Array

A Halbach array consists of a series of uniformly magnetized magnets arranged continuously so that their dipole moments exhibit a discrete rotation sequence [1]. In this section, a two-dimensional Halbach array pattern is considered. This simplified framework offers key insight into the capabilities of the array for the applications of interest. The magnetization pattern of the 2D Halbach array is given by

$$\boldsymbol{M}_0 = M_0 \left[f(x)\boldsymbol{u}_x + g(x)\boldsymbol{u}_y \right] \tag{12}$$

where $f(x)$ and $g(x)$ are two respectively odd and even $x-$periodic functions, such that $f(x) = -f(-x)$, $g(x) = g(-x)$, and

$$\begin{array}{llll} f(x) = 0, & g(x) = 1, & \text{if} & 0 < x < \lambda/8, \\ f(x) = -1, & g(x) = 0, & \text{if} & \lambda/8 < x < 3\lambda/8, \\ f(x) = 0, & g(x) = -1, & \text{if} & 3\lambda/8 < x < \lambda/2. \end{array} \tag{13}$$

Following Fig. 1, λ denotes the spatial frequency of the array, a the width of each magnet, and b its height. The array is composed of individual magnets with magnetization M_0 located at a distance h from a ferrofluid layer of thickness δ. The gravity acceleration g acts with an angle α with respect to the vertical. A reference system defined along ($\boldsymbol{u}_x$) and normal ($\boldsymbol{u}_y$) to the magnetized layer is employed in this report, with x and y denoting its Cartesian coordinates.

The Halbach array is a discrete approximation to the continuous Mallinson configuration, which consists of a magnetized medium in a planar structure with a rotating magnetization pattern [3]

$$\boldsymbol{M}_0 = M_0 \left[-\sin(kx)\boldsymbol{u}_x + \cos(kx)\boldsymbol{u}_y \right], \tag{14}$$

with $k = 2\pi/\lambda$ being the wavenumber of the magnetic pattern.

1.2.3 External Magnetic Field

The magnetic field produced by a Halbach array in the absence of magnetized media, subsequently defined as *external* magnetic field, derives from the scalar magnetic potential Φ_m^H. The codes employed in this report employ different approximations to the computation of the field, depending on their scope and final intent.

Analytical Approximation: The periodic vector function in Eq. 12 can be expressed in terms of a Fourier expansion

$$\boldsymbol{M}_0 = \frac{2\sqrt{2}M_0}{\pi} \sum_{i=1}^{\infty} \frac{1}{(2i-1)} \, \boldsymbol{m}_{2i-1}(x), \tag{15}$$

where

$$\boldsymbol{m}_n(x) = \begin{cases} (-1)^{\frac{n+3}{4}} \left[\sin(k_n x)\boldsymbol{u}_x - \cos(k_n x)\boldsymbol{u}_y\right], & \text{if } \; n = 1, 5, 9, \cdots \\ \\ (-1)^{\frac{n+5}{4}} \left[\sin(k_n x)\boldsymbol{u}_x + \cos(k_n x)\boldsymbol{u}_y\right], & \text{if } \; n = 3, 7, 11, \cdots \end{cases} \tag{16}$$

with $k_n = 2n\pi/\lambda$ denoting the wavenumber of the corresponding spatial harmonic. The magnetic scalar potential on $y > -h$ resulting from this configuration is of the form

$$\Phi_m^H(x, y > -h) = \sum_{i=1}^{\infty} (-1)^{i-1} \, \Phi_{(4i-3)}^H, \tag{17}$$

with

$$\Phi_n^H = \frac{2\sqrt{2}M_0}{n\pi \; k_n} \, e^{-k_n h}(1 - e^{-k_n b})e^{-k_n y}\cos(k_n x). \tag{18}$$

Consequently, the external magnetic field produced by a Halbach array becomes

$$\boldsymbol{H}_{_H}(x, y > -h) = -\nabla\Phi_m^H = \sum_{i=1}^{\infty} (-1)^{i-1} \, \boldsymbol{H}_{(4i-3)}(x, y), \tag{19}$$

with

$$\boldsymbol{H}_n(x, y > -h) = \frac{H_{0n}}{n} \, e^{-k_n y} \left[\sin(k_n x)\boldsymbol{u}_x + \cos(k_n x)\boldsymbol{u}_y\right], \tag{20}$$

and where

$$H_{0n} = \frac{2\sqrt{2}\, M_0}{\pi} \; M_0 e^{-k_n h}(1 - e^{-k_n b}). \tag{21}$$

Conversely, the Mallinson configuration leads to a much simpler external magnetic field

$$\boldsymbol{H}_0(x, y > -h) = H_0 e^{-ky} \left[\sin(kx) \; \boldsymbol{u}_x + \cos(kx) \; \boldsymbol{u}_y\right] \tag{22}$$

in the $y > -h$ region, with $H_0 = M_0 e^{-kh}(1 - e^{-kb})$.

Numerical Approximation: Although the analytical external field approximations are employed in some of the codes, the study of non-trivial Halbach configurations (e.g. curved Halbach arrays or point disturbances) can only be achieved by the numerical simulation of a superposition of uniformly magnetized magnets. Towards that end, the magnetic field of each unit is computed by simulating the *equivalent magnetization current* $\boldsymbol{K}_m = \boldsymbol{n} \times [\boldsymbol{M}]$ at the lateral walls of each block magnet [9].

1.2.4 Interface Deformations

As indicated in Sec. 1.2.1, the study of the deformations of the ferrofluid interface exposed to the magnetic field produced by a Halbach array requires solving the coupled fluid-magnetic problem summarized in Eq. 10. The derivation of results will be the subject of a future publication. However, the amplitude ε of the $2k$ ferrofluid wave arising sufficiently far away from the array to avoid $4k$ frequency waves associated with higher-order harmonics and sufficiently close to avoid $1k$ edge effects is

$$k\varepsilon \approx \frac{\xi}{4}\left[1-\frac{2}{5}\beta e^{-4k(h+\delta)}\right]\left[1+\frac{4\sigma k+\rho g/k}{\mu_0 M_s H_{01} e^{-k\delta}}-\beta e^{-4k(h+\delta)}\right]^{-1} \tag{23}$$

where $\xi = M_s e^{k\delta}/H_{01} \ll 1$, $\beta = (1-e^{-5kb})/(1-e^{-kb})$, and M_s is the saturation magnetization of the ferrofluid. This expression considers volume and surface magnetic forces, gravity, surface tension, and the first Harmonic of the Halbach discretization presented in Eq. 15.

During the testing of a 0.25 × 0.25 m^2 Halbach array prototype, it was observed that the 2k ripple on a commercial ferrofluid was a factor of 3-5 greater than expected [10]. This discrepancy was attributed to density variations in the ferrofluid which couple to and reinforce the magnetic field strength variations due to the 2k ripple. If ferrofluid density variations are included in the model, then the saturation magnetization $M_s(x,y)$ depends on the concentration of particles $n(x,y)$ through[2]

$$M_s(x,y) = \frac{m_{\text{dip}}}{\mu_0} n(x,y) \tag{24}$$

with m_{dip} identifying the magnetic dipole moment of the nanoparticles composing the ferrofluid, and $n(x,y)$ the nanoparticle density function. Based on the force distribution, and assuming $M(x,y) \approx M(x)$, the saturation curve can be approximated as

$$M_s(x) = M_s\left\{1+\frac{\Delta n}{2n_0}\left[\left(\frac{1}{2}-\kappa\right)-\cos(2kx)+\left(\frac{1}{2}+\kappa\right)\cos(4kx)\right]\right\}, \tag{25}$$

where Δn is the increment in nanoparticle density at the concentration peaks with respect to the average n_0, M_s is the baseline saturation magnetization, and κ is a heuristic parameter that allows modeling the redistribution of magnetic particles. Considering that $\kappa \to -1/2$, so that only the first harmonic has a significant effect on the particle redistribution, and making additional assumptions involving the operational environment of the ferrofluid layer, the surface mid-frequency error described by Eq. 23 becomes

$$k\varepsilon \approx \Gamma\left\{\frac{\Delta n}{2n_0}+\frac{\xi}{4}\left\{1-\frac{\Delta n}{n_0}F_1(\chi)-\frac{1}{2}\left(\frac{\Delta n}{n_0}\right)^2\left[1+F_2(\chi)-e^{-k\delta}\right]\right\}\right\}, \tag{26}$$

with

$$\Gamma\left(\sigma,\rho,g,M_s,H_0,\delta,\chi\right) = \left\{1+\frac{4\sigma k+\rho g/k}{\mu_0 M_s H_0 e^{-k\delta}}+\frac{\Delta n}{2n_0}\left[1+\frac{\xi}{2}e^{-k\delta}\left(1+\frac{\Delta n}{2n_0}\right)\right]\right\}^{-1}. \tag{27}$$

$F_{1,2}(\chi)$ are heuristic parameters whose value depends on how the redistribution process of magnetic particles affects the magnetization of the ferrofluid. As a first approximation, it can be estimated that their values are in the ranges $1/\chi < F_1(\chi) < 2/\chi$, and $0 < F_2(\chi) = 2/\chi$. Even though Eq. 26 is the result of multiple first-order approximations to the ferrohydrodynamic behavior of the system, it shows that variations in the ferrofluid nanoparticle concentration can have a significant impact on the mid-frequency error ε, as they generate additional terms that can easily overcome error estimations from Eq. 23.

1.2.5 Numerical calculation of ferrofluid body force potential

The numerical evaluation of the potential field described by Eq. 8 requires integrating the magnetization function. The constitutive relation in Eq. 7 relates the ferrofluid magnetization M and magnetic field H, and can be modeled, in first-order approximation, through the Langevin function [2]

$$M(H) = M_s L(H), \tag{28}$$

where

$$L(H) \equiv \coth(\gamma H) - \frac{1}{\gamma H} \tag{29}$$

and γ is some arbitrary constant. Because the initial magnetic susceptibility χ is defined as the slope of the $M(H)$ curve when $H \to 0$, γ can be found as

$$\gamma = \frac{3\chi}{M_s}. \tag{30}$$

Finally, the total body force potential in Eq. 8 is expressed as

$$\Pi = gz + \Pi_m = gz - \frac{\mu_0 M_s}{\rho\gamma}\left(\ln(1 - e^{-2|\gamma H|}) - \ln|\gamma H| + |\gamma H| - \ln 2\right), \tag{31}$$

which, again, assumes a constitute relation of the form denoted by Eq. 28.

1.2.6 Rosensweig Instability

The Rosensweig instability is the spontaneous formation of a regular pattern of peaks and valleys on the surface of a ferrofluid when it is subjected to a strong external magnetic field. The instability occurs when the ferrofluid reaches the critical magnetization level M_c [2]. For the optical designs considered in this report, preventing the Rosensweig instability becomes a hard constraint. In the case of nonlinear media exposed to an oblique external magnetic field, M_c can be computed as [2]

$$M_c^2 = \frac{2}{\mu_0}\left(1 + \frac{1}{r_0}\right)\left[\sqrt{\Delta\rho g\sigma} + \frac{\mu_0(1 - r_0)^2}{2(1 + r_0)} H_x^2\right], \tag{32}$$

where $\Delta\rho \equiv |\rho_1 - \rho_2|$ is the density difference across the interface, H_x is the magnetic field component tangent to the ferrofluid surface, and r_0 is the geometric mean of the chord and tangent magnetic permeabilities

$$r_0 = \frac{\sqrt{\mu_c\,\mu_t}}{\mu_0}, \tag{33a}$$

$$\mu_c \equiv \frac{B}{H}, \tag{33b}$$

$$\mu_t \equiv \left(\frac{dB}{dH}\right)\Big|_H. \tag{33c}$$

Implementing the Langevin curve in Eq. 29 and considering Eqs. 33 the geometric mean becomes

$$r_0 = \sqrt{\left(\frac{M_s L(H_0)}{H_0} + 1\right)\left[1 + M_s\left(\frac{1}{\gamma H_0^2} - \gamma\,\mathrm{csch}^2(\gamma H_0)\right)\right]}. \tag{34}$$

In general, the design space needs to satisfy $M < M_c$ for the entire ferrofluid domain.

1.3 What's Included?

The codes outlined in this document can be used to characterize the properties of Halbach-based magnetic liquid mirrors, both for design space studies and for design optimization. Each code includes a brief description at the beginning of its section, followed by the assumptions made in the model and key outputs. Three tables are given for each code, corresponding to the descriptions of the code blocks in the main file, the interactions with dependencies, and function inputs and outputs.

1. Design space mapping tools (Sec. 2) are used to decide on Halbach array size and ferrofluid properties and configuration. This code provides an early trade space analysis on the technology and considers the full ferrohydrostatic framework developed in Sec. 1.2.
2. Two-dimensional flat Halbach array simulations (Sec. 3) are the basis for studies of single-magnet disturbances, edge effects, tilting, actuation mechanisms, and others. The code adopts the simplified equipotential framework summarized by Eq. 11.
3. Three-dimensional spherical Halbach array simulations (Sec. 4) provide a first-order analysis of ferrofluid tilting effects for a spherical mirror substrate, informing the design of actuation systems. The code exploits the decoupling between the simplified equipotential framework by Eq. 11 and the full-physics framework in Sec. 1.2.4.
4. 3D Halbach array simulations (Sec. 5) are the most computationally intensive simulations outlined in this document, as they adopt the Finite Element Method (FEM) to get a full magnetic equipotential map of a 3D curved Halbach array. This framework will become particularly useful during the construction and tuning of large-scale 3D prototypes.
5. The passive/active 2D Halbach simulation (Sec. 6) provides a final framework to study engineering solutions to control the mid-frequency wavefront error and global deformation of the interface during tilting.
6. Code dependencies (Sec. 7) are also included for completeness.

1.4 Required Software

1. MATLAB (ver. 2023B) (Codes 2–7)
   (a) Curve Fitting Toolbox (ver. 3.8) (Codes 3,4)
   (b) Optimization Toolbox (Code 4)
2. COMSOL Multiphysics 6.2 (Code 5)
   (a) AC/DC Module (Code 5)
   (b) Comsol-Matlab LiveLink (Code 5)

1.5 Acknowledgements

This report was prepared under the DARPA Contract FA237724CB011 for the DARPA Zenith Phase I Program HR0011366236.

2 Design Space Mapping

2.1 Purpose

The mid-wavefront error induced by the Halbach array on the ferrofluid, described by Eq. 23, defines the ability of different magnetic configurations to produce the desired optical surface. As such, design space mapping software is needed to determine which combinations of magnet sizes, ferrofluid properties, and design specifications are ideal. Two codes were developed to help with this - one to plot mid-wavefront error versus saturation magnetization and ferrofluid height and another to plot mid-wavefront error versus magnetic wavelength and height-wavelength ratio. These properties are the main input parameters for the simulation of the mid-wavefront error, and as such the full four-dimensional design space is explored.

The mid-wavefront error vs. saturation magnetization and ferrofluid height plotting code generates multiple plots of the mid-wavefront error, magnetic force, ξ, and the ξ, force, and Rosensweig instability constraints for different magnet sizes. Additionally, the point with the lowest error within the allowed region is selected. This code's structure is documented in tables 1-3, and the main file is "roughness_vs_error_plots.m." Fig. 2 shows an example of the resulting plot.

The mid-wavefront error vs. magnet wavelength and height-wavelength ratio plotting code shows the properties of the lowest-error allowed point in the prior code as the magnet wavelength and height are changed. It generates a plot of the mid-wavefront error, ξ, magnet count per inch, ferrofluid saturation magnetization, and the ξ, Rosensweig instability, and h/λ constraints. This code's structure is documented in tables 4-6, and the main file is "plot_E.m." Fig. 3 shows an example of the resulting plot.

2.2 Assumptions

Both sets of code share an assumption set, as they use the same theoretical framework to calculate design space properties, and merely show different cross-sections of it.

1. The Halbach array is large compared to the wavelength. It is thus approximated as infinite, and edge effects are not considered.
2. The radius of curvature of the Halbach array is much larger than the wavelength. Therefore, it is approximated as flat.
3. The constitutive equation of the ferrofluid is interpolated from the Ferrotec's water-based ferrofluids catalog.
4. Taylor series terms of the Halbach array's magnetic field of the tenth order or above are neglected.
5. The ratio of the ferrofluid height to magnetic wavelength (h/λ) greater than 0.1
6. The ratio of saturation magnetization to magnetic field strength (ξ) is much smaller than 1

2.3 Code Structure

Table 1: Code structure for mid-wavefront error vs. saturation magnetization and ferrofluid height plotting

Section	Lines	Description	I/O
Introduction	1-9	Definition of code objectives	No
Code configuration	10-13	Visual and numerical options for plotting	Yes
Constants	14-17	Physical constants needed for the evaluation of the mid-wavefront error	Yes

Magnetic Curve Interpolation	18-32	Determination of ferrofluid parameters from Ferrotec data	No
Parameters	33-44	Additional ferrofluid and Halbach array properties, and limits on the ranges of independent variables	Yes
Variant parameters	45-51	Parameters which must be defined as arrays corresponding to variable inputs	No
Magnet properties for-loop	52-61	Iteration through the magnets being observed, and generation of figure titles	No
Intermediate results	62-69	Results which are necessary for the calculation of force and wavefront error	No
Surface force	70-73	Calculation of the mass-specific magnetic force on the ferrofluid, normalized to gravity	No
Surface mid-wavefront error	74-78	Computation of the surface mid-wavefront error from previous results	No
Rosensweig instability	79-86	Determination of the critical magnetization and the error margin between it and the ferrofluid magnetization	No
Plot generation	87-167	Plot generation for each magnet	No
Plot formatting	168-174	Plot formatting to LGST standard	No

Table 2: Descriptions for functions used in mid-wavefront error vs. saturation magnetization and ferrofluid height plotting

Function name	Description
createFit_RhoVsMs	Creates a MATLAB curve fitting to the density and saturation magnetization data of the ferrofluid
createFit_Chi0VsRho	Creates a MATLAB curve fitting to the initial magnetic susceptibility and density data of the ferrofluid
megacontour	Plots a solid contour line representing a constraint on the problem on the design space, along with a dashed line representing which side of the constraint is feasible

Table 3: I/O of functions used in mid-wavefront error vs. saturation magnetization and ferrofluid height plotting

Function name	I/O	Comments
createFit_RhoVsMs	[Ms, rho];[fitresult, gof]	Ms and rho are the ferrofluid saturation magnetization and density, respectively
createFit_Chi0VsRho	[rho, chi0];[fitresult, gof]	rho is ferrofluid density as before, and chi0 is initial magnetic susceptibility

megacontour	[x, y, Z, c0, c1, color];[bpoint]	x, y, and Z are the 2D contour plotting arrays, c0 is the constraint, and c1 is a point on the correct side of the constraint being plotted. color is the desired color of the diagram, and bpoint is the highest point found within the design region.

Table 4: Code structure for mid-wavefront error vs. magnet wavelength and height-wavelength ratio plotting

Section	Lines	Description	I/O
Introduction	1-9	Definition of code objectives	No
Code configuration	10-12	Numerical options for plotting	Yes
Parameters	13-22	Additional ferrofluid and Halbach array properties, and limits on the ranges of independent variables	Yes
Constants	23-26	Physical constants needed for the evaluation of the mid-wavefront error	Yes
Magnetic Curve Interpolation	27-41	Determination of ferrofluid parameters from Ferrotec data	No
Variant parameters	42-46	Parameters which must be defined as arrays corresponding to variable inputs	No
Result generation	47-61	Generates error, saturation magnetization, ξ, and the wavefront error, with progress reports produced in the console	No
Plot generation	62-111	Generating the result plots	No
Plot formatting	112-135	Plot formatting to LGST standard	No

Table 5: Descriptions for functions used in mid-wavefront error vs. magnet wavelength and height-wavelength ratio plotting

Function name	Description
createFit_RhoVsMs	Creates a MATLAB curve fitting to the density and saturation magnetization data of the ferrofluid
createFit_Chi0VsRho	Creates a MATLAB curve fitting to the initial magnetic susceptibility and density data of the ferrofluid
megacontour	Plots a solid contour line representing a constraint on the problem on the design space, along with a dashed line representing which side of the constraint is feasible
find_E	Finds the minimum saturation magnetization to get a magnetic force of 98.1 m/s^2 on the ferrofluid, and the wavefront error and other design considerations associated with it
find_GandE	Finds the magnetic force based on a given design configuration; used by find_E to optimize the saturation magnetization

Table 6: I/O of functions used in mid-wavefront error vs. magnet wavelength and height-wavelength ratio plotting

Function name	I/O	Comments
createFit_RhoVsMs	[Ms, rho];[fitresult, gof]	Ms and rho are the ferrofluid saturation magnetization and density, respectively
createFit_Chi0VsRho	[rho, chi0];[fitresult, gof]	rho is ferrofluid density as before, and chi0 is initial magnetic susceptibility
megacontour	[x, y, Z, c0, c1, color];[]	x, y, and Z are the 2D contour plotting arrays, c0 is the constraint, and c1 is a point on the correct side of the constraint you want to plot. color is the desired color of the diagram
find_E	[lambda, hratio , RhovsMs_cfit , Chi0vsRho_cfit, params]; [e, Ms, xi, keps, inst]	Lambda is λ, hratio is the height ratio of the ferrofluid to the magnets, the fit variables are interpolants, and params are the parameters. Ms, xi, and keps are $M_s, \xi, k\epsilon$, inst is positive when the Rosenswieg instability becomes significant , and e is the error.
find_GandE	[lambda, hratio , Ms , RhovsMs_cfit , Chi0vsRho_cfit, params]; [f_vol_y_g, Roughness , xt, keps, inst]	This function uses the same variables as the one above.

2.4 Representative Outputs

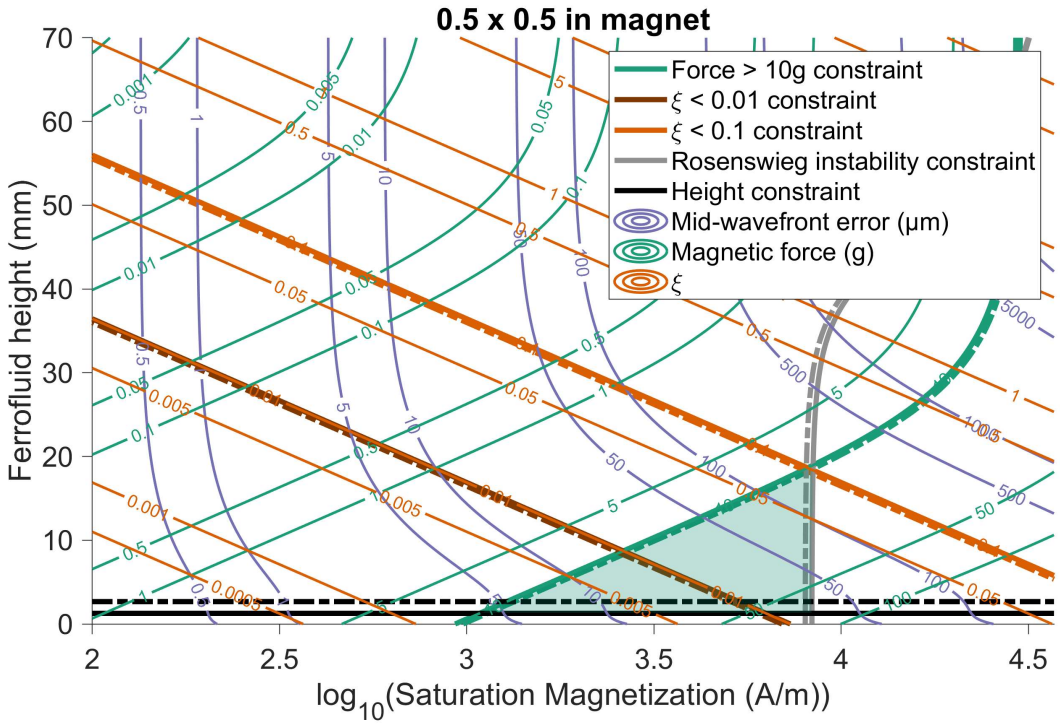

Fig. 2: Mid-wavefront error vs. saturation magnetization and ferrofluid height

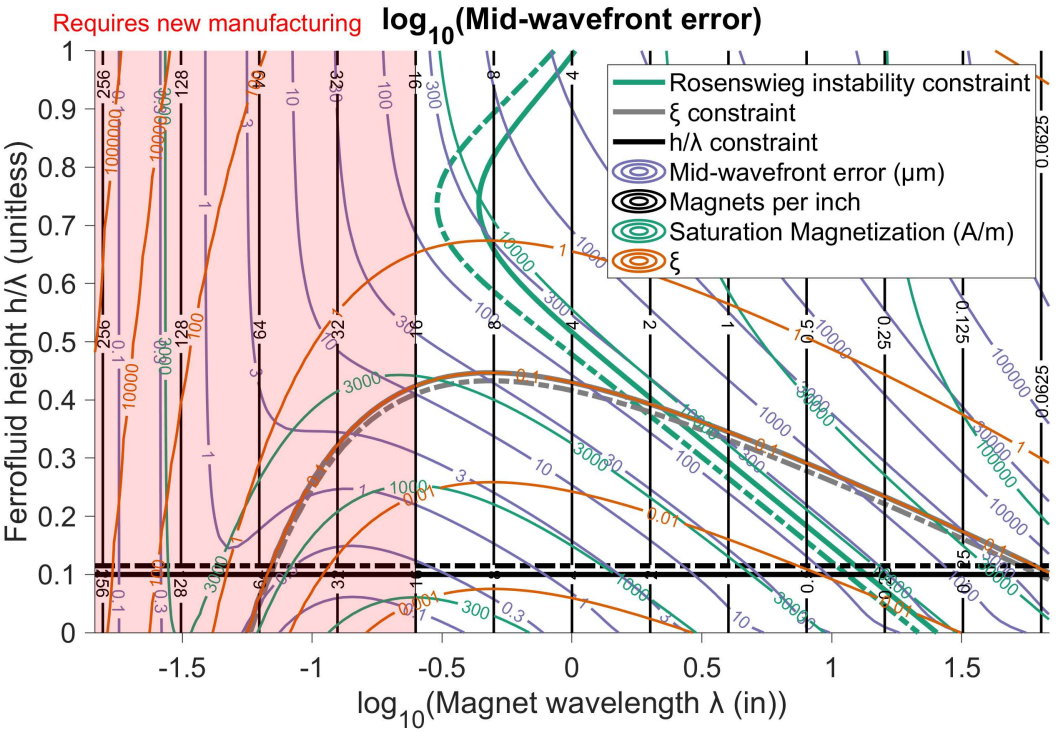

Fig. 3: Mid-wavefront error vs. magnet wavelength and height-wavelength ratio

3 2D Flat Halbach Array

3.1 Purpose

This code is used to compute the magnetic flux density, magnetic potential, and the kelvin body force distribution of a 2D flat Halbach array as a function of the Halbach array's parameters. The code approximates the magnets as infinite current sheets going in and out of the side of the magnet and only accounts for the magnetic potential.

3.2 Assumptions

1. Only magnetic forces are accounted for.
2. Magnets are modeled as infinite current sheets going in and out of both sides of the magnet (see Sec. 1.2.3).
3. The ferrofluid properties are interpolated from the data of existing FerroTec water-based ferrofluids.
4. The ferrofluid is assumed to follow the Langevin magnetization curve.

3.3 Code Structure

Table 7: Code structure for 2D Flat Halbach Array main script

Section	Lines	Description	I/O
Halbach parameters	19-26	Definition of Halbach array properties	Yes
Simulation parameters	29-30	Physical constants	Yes
Storage of data	34-42	Storage of parameters in structure	No
Magnet placement	45-49	Positioning of magnet in Cartesian frame	No
Magnetization direction	52-56	Position of magnetization direction	No
Simulation definition for B field	59-72	Simulation range for B field computation	No
Storage of data	75-76	Storage of simulation parameter in structure	No
B field Computation	80-84	Computation of Magnetic Flux field	No
Kevin Body Force computation	90-116	Computation of Kelvin Body Force distribution	No
Plotting of the B field	120-138	Representation of B field distribution	Yes
Plotting of equipotential map	143-166	Representation of equipotential line	Yes
Plotting of KBF distribution	173-190	Representation of Kelvin Body Force distribution	Yes
Plot Formatting and Storage	193-213	Plot standardization and storage	Yes

Table 8: Descriptions for functions used for 2D Flat Halbach Array

Function name	Description
get_Rho_Chi0_Phi	Calculates Ferrofluid properties based on interpolation of Ms
createFit_PhiVsMs	Curve-fits ϕ and M_s of Ferrofluid
createFit_Chi0VsPhi	Curve-fits χ_0 and ϕ of Ferrofluid
createFit_RhoVsPhi	Curve-fits ρ and ϕ of Ferrofluid
calculatingB	Computes the two magnetic flux density vector components in 2D.
magnetization	Calculates ferrofluid magnetization from the magnetic field
Kelvin_H	Calculates the Kelvin Body force from magnetic field H
Plot_magnets	Plots magnet shape on top of existing plots

Table 9: I/O of Functions used for 2D Flat Halbach Array

Function name	Input	Output
get_Rho_Chi0_Phi	Ms	[rho,chi0,phi]
createFit_PhiVsMs	[Ms_data, phi_data]	[fitresult, of]
createFit_Chi0VsPhi	[phi_data, Chi0_data]	[fitresult, of]
createFit_RhoVsPhi	[phi_data, rho_data]	[fitresult, of]
calculatingB	[params,h,w,X,Y,theta,r0]	[Bx,By]
magnetization	[H,params]	[M]
Kelvin_H	[M_vec, Hx,Hy,params]	[Fk_x,Fk_y,Fk]
Plot_magnets	[theta,w,h,r0,cover]	N/A

3.4 Representative Outputs

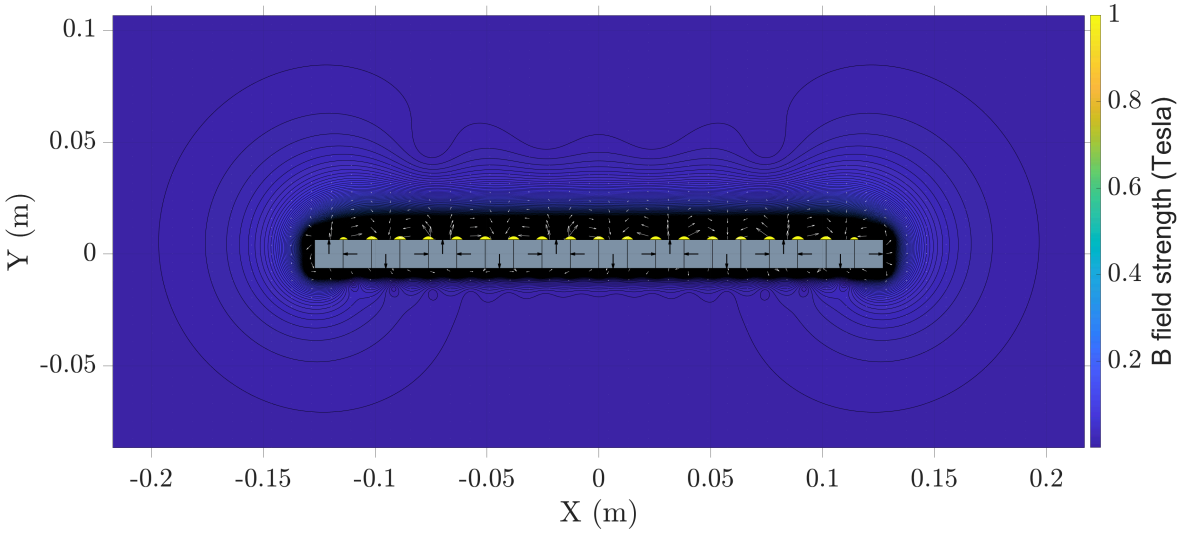

Fig. 4: Magnetic flux density map of a 2D flat Halbach array

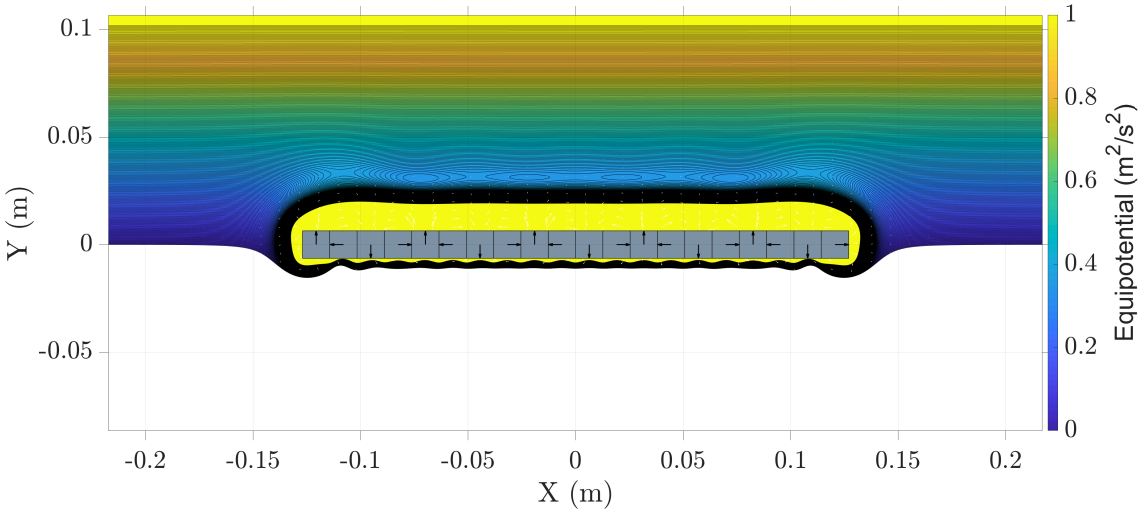

Fig. 5: Equipotential line Map of a 2D flat Halbach array

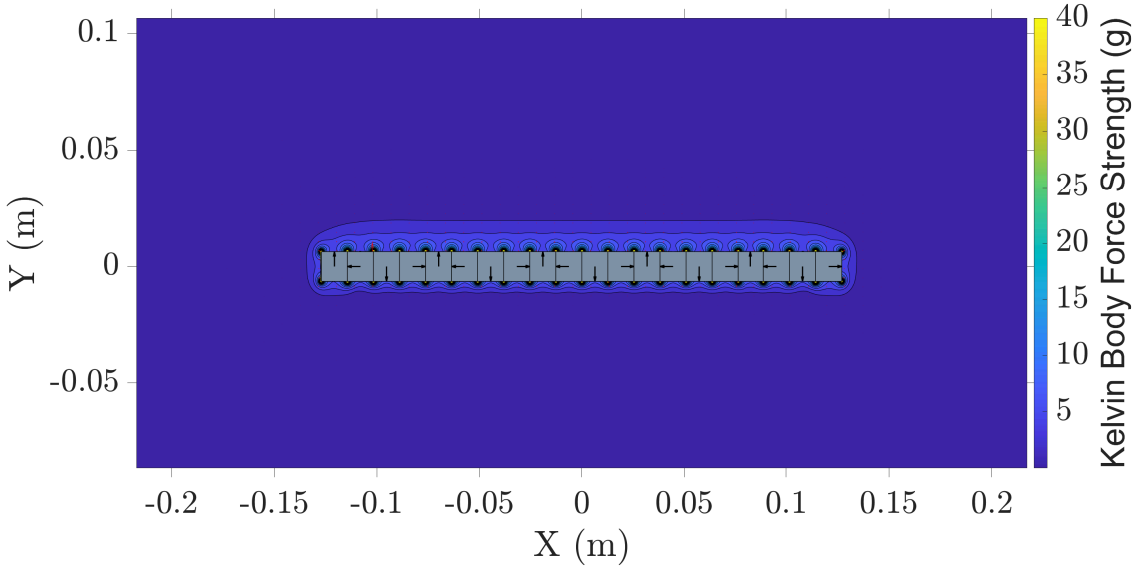

Fig. 6: Kelvin Body Force Map of a 2D flat Halbach array

4 3D Spherical Global Tilting

4.1 Purpose

The 3D spherical global tilting code determines the shape of the equipotential ferrofluid surface on a three-dimensional spherical Halbach array as a function of the tilting angles and the ferrofluid properties. Following the superposition principle, the full-physics solution of the surface wave (Sec. 1.2.4) is added to the equipotential line. This informs the design of active control mechanisms through optical characterization. Both 2D and 3D plots of the ferrofluid surface are generated, and superimposed on the dish and Halbach array outline.

The ferrofluid surface is calculated by varying the central height of the ferrofluid until the ferrofluid volume (generated by integrating the equipotential line corresponding to the chosen central point) matches that without tilting.

4.2 Assumptions

1. The ideal Mallinson magnetic field described by Eq. 22 is assumed.
2. Second-order magnetic field bending effects associated with the curved array are omitted.
3. Magnetic edge effects are omitted.
4. Contact line effects are omitted.
5. The ratio of the ferrofluid height to magnetic wavelength (h/λ) is smaller than 0.1.
6. The ratio of saturation magnetization to magnetic field strength (ξ) is much smaller than 1.

4.3 Code Structure

Table 10: Code structure for 3D Spherical Global Tilting

Section	Lines	Description	I/O
Introduction	1-28	Definition of code objectives	No
Code configuration	30-33	Clearing variables, adding path to functions etc.	No
Fluid parameters	35-43	Ferrofluid and mirror surface properties	Yes
Halbach parameters	45-54	Halbach array and magnet properties	Yes
Halbach derived parameters	56-58	Additional experimental setup parameters	No
Constants	60-62	Physical constants used in the model	No
Computation fidelity	65	Fidelity of mesh	Yes
Constitutive equation	68	Interpolation of ferrofluid properties from Ms	No
Store parameters	71-94	Storage of necessary parameters	No
Mesh	98-102	Generation of mesh for the ferrofluid surface	No
Surface profiles definition	106-111	Definition of dish and target ferrofluid profile	No
Volume evaluation	114-115	Calculation of ferrofluid half volume	No
Coordinate transformation	118-120	Transformation of coordinate frames	No
Definition of magnetic field	123-133	Evaluation of the magnetic field and potential	No
Save magnetic params	136-149	Stores newly generated parameter	No
Introduction of surface differential	151-159	Explanation of surface differential approach	No
Zenith Interface	161-165	Calculation of zenith interface	No
Outer region adjustment	167-169	Removing outer region	No
Differential height	171-175	Calculating the height difference	No

Gravity potential update	177-181	Updating gravity and overall potential under tilt	No
Interface shape minimization problem	183-191	Finds the interface while maintaining volume	No
Surface mid-freq oscillations	193-199	Calculating the new mid-frequency oscillation	No
Represent interface	205-208	Plotting of the resulting ferrofluid interface	No
Represent dish	210-213	Plotting of the dish surface	No
Represent Halbach	216-218	Plotting of the resulting Halbach array	No
Plot figure	220-226	Plotting of the surface and substrates	No
Plot figure sideview	231-248	Plotting of interface and substrates in 2D	No
Write data to text file	251-253	Printing data for later use	No
Plot Formatting	256-262	Plot standardization	No

Table 11: Descriptions for functions used in 3D Spherical Global Tilting

Function name	Description
createFit_RhoVsPhi	Creates a MATLAB curve fitting to the density and solute volume percentage data of the ferrofluid
createFit_PhiVsMs	Creates a MATLAB curve fitting to the solute volume percentage and saturation magnetization data of the ferrofluid
createFit_Chi0VsPhi	Creates a MATLAB curve fitting to the initial magnetic susceptibility and solute volume percentage data of the ferrofluid
get_Rho_Chi0_Phi	Interpolates the ferrofluid density, initial magnetic susceptibility, and solute volume percentage from saturation magnetization
magpot	Computes the magnetic potential and its derivatives in the horizontal and vertical directions at the input points
magnetization	Calculates ferrofluid magnetization from the magnetic field
midfreq_oscillations	Calculates the mid-wavefront error
gridinterp_Pi_m	Does a 3-dimensional interpolation of the magnetic potential
residuals_setPI	Determines the residual potential for the 3D equipotential interface
residuals_setV	Computes the residual volume of the interface

Table 12: I/O of functions used in 3D Spherical Global Tilting

Function name	I/O	Comments
createFit_RhoVsPhi	[phi_data, rho_data] ;[fitresult, gof]	phi_data and rho_data are the ferrofluid solute volume percentage and density, respectively.
createFit_PhiVsMs	[Ms_data, phi_data] ;[fitresult, gof]	Ms_data and phi_data are the ferrofluid saturation magnetization and solute volume percentage, respectively.
createFit_Chi0VsPhi	[phi_data, Chi0_data] ;[fitresult, gof]	phi_data and Chi0_data are the ferrofluid solute volume percentage and initial magnetic susceptibility, respectively.

get_Rho_Chi0_Phi	[Ms] ;[rho,chi0,phi]	Ms,rho,chi0,and phi are the ferrofluid saturation magnetization, density, initial magnetic susceptibility, and solute volume percentage.
magpot	[x,z,params] ;[Pi_m, dPi_m_dx, dPi_m_dz]	x and z are the distance from the center of the array and the height, params is the MATLAB structure containing general system parameters, Pi_m is the magnetic potential, and dPi_m_dx and dPi_m_dz are the magnetic potential's derivatives in x and z, respectively.
magnetization	[H,params];[M]	H is the magnetic field strength, params is the MATLAB structure containing general system parameters, and M is the ferrofluid magnetization.
midfreq_oscillations	[x,f,params];[epsilon]	x and f are the horizontal position and radial error of the ferrofluid surface. params is the MATLAB structure containing general system parameters, and epsilon is the total ferrofluid surface error.
gridinterp_Pi_m	[x_m,z_m,H_m,params] ;[Pi_m]	x_m, z_m, and H_m are arrays corresponding to the horizontal and vertical positions, and the magnetic field strength over a grid. params is the MATLAB structure containing general system parameters, and Pi_m is an interpolant of the magnetic potential.
residuals_setPI	[Z, z0, params];[res]	Z is the vector of state (elevations of (x,y) points) and z0 the target height at (0,0) params is the MATLAB structure containing general system parameters, and res is the vector of potential residuals
residuals_setV	[z0, params];[Vres]	z0 is the target height at (0,0) params is the MATLAB structure containing general system parameters, and Vres is the interface residual volume.

4.4 Representative Outputs

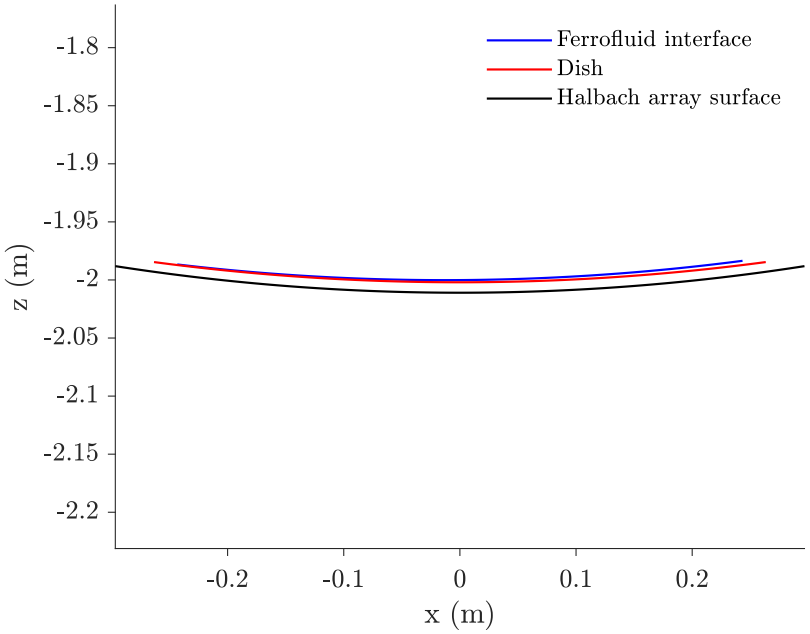

Fig. 7: Shape of the ferrofluid interface and relevant surfaces for the 3D spherical analytical Halbach array

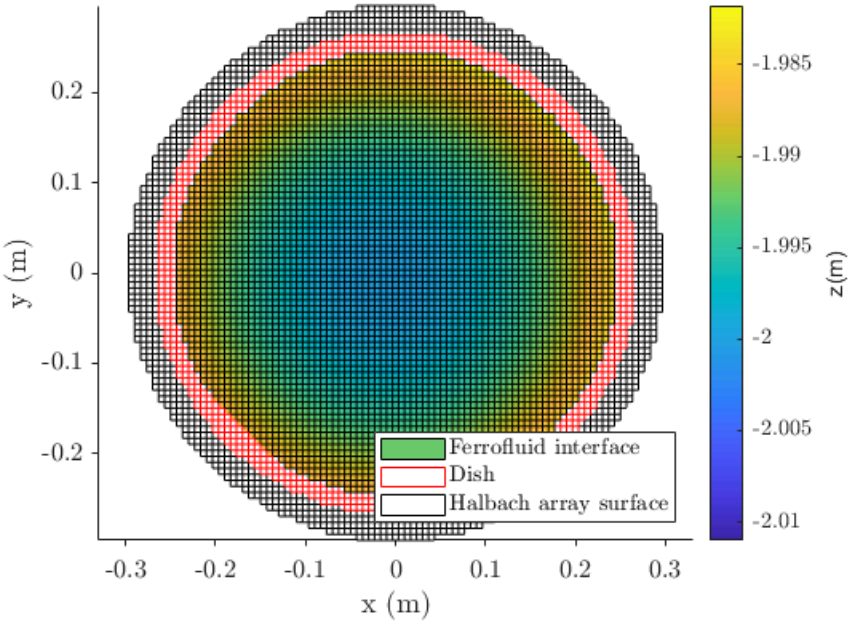

Fig. 8: Surface mid-frequency oscillation map for the 3D spherical analytical Halbach array

5 3D Comsol Simulation

5.1 Purpose

The most computationally intensive model of the Halbach array liquid mirror telescope is the full three-dimensional (3D) simulation. The 3D geometry of block magnets has no closed-form solution and thus is simulated through FEA in COMSOL Multiphysics 6.2. The model adopts the equipotential theory summarized in Eq. 11.

The COMSOL-MATLAB API (LiveLink) connects MATLAB with the COMSOL server so that all the settings in the COMSOL simulation are controlled through a MATLAB script. The simulation first computes the flux density field created by the Halbach Array and uses the results to calculate the ferrofluid body force potentials from the combined gravitational and magnetic body forces further. The simulation also calculates the electromagnetic forces and torques experienced by each magnet at its geometric center when forming the Halbach Array. Finally, the script loads the resulting plots from the COMSOL model and plots them in MATLAB. In addition, this version allows the user to add a passive corrector above the Halbach Array to investigate passive wavefront correction strategies.

5.2 Assumptions

1. Magnetic and gravitational forces are considered.
2. Torque is calculated relative to magnet centers.
3. Every magnet has the same uniform magnetization, matching the N-52 neodymium designation.
4. The ferrofluid properties are interpolated from the data of existing FerroTec water-based ferrofluids.
5. The ferrofluid is assumed to follow the Langevin magnetization curve to calculate the body force potential.

5.3 Code Structure

Table 13: Code structure for 3D Halbach Array COMSOL Simulation

Section	Lines	Description	I/O
Introduction	1-15	Introduction of the main script	No
Add path & load pre-built model	16-20	Add relevant path and load the pre-built model	Yes
Initialize the design parameters	21-65	Initialize the all the design parameters and switches	Yes
Build the Geometries	66-177	Use a For loop to place and orient each individual magnet and build a magnetic passive corrector geometry.	No
Adding materials, meshes, physics	178-286	Assign materials, meshes, and physics to each individual magnet and the magnetic passive corrector	No
Run study	287-289	Run the study	Yes
Postprocessing	290-538	Extract data from the COMSOL model, Plot the results.	Yes
Save and open the model	539-546	Save the studied model and open the model in COMSOL GUI for inspection	Yes

Table 14: Descriptions for functions used in 3D Halbach Array COMSOL Simulation

Function name	Description
calc_PI	Calculates magnetic potential
comsolinit	COMSOL LiveLink initialization script
extractpoints	Extracts and sorts the COMSOL output to generate a contour.
RotatingHB_magnetPose	Determines the positions and orientations of the magnets for a curved Halbach array where the magnets face the normal vector of the curve.
StepHB_magnetPose	Determines the positions and orientations of the magnets for a Halbach array that, despite being curved, has the individual magnets aligned.

Table 15: I/O of functions used in 3D Halbach Array COMSOL Simulation

Function name	I/O	Comments
calc_PI	[Z, H_norm];[PI]	Z is height and H_norm is the strength of the magnetic field
comsolinit	[];[]	No I/O
extractpoints	[p,sphere_center, distance2SphereCenter] ;[p_new]	P_new is the new contourline, p is the old contourline, sphere_center is the focal point, and distance2SphereCenter is the radius.
RotatingHB_magnetPose	[a,b,n_mag,half_range] ;[r_mag,k,psi,Br_orient_strArr]	a and b are parabola properties, n_mag is the number of magnets in one direction, and half_range is the last magnet's location in each quadrant. r_mag is magnet position,k and psi are the rotation instructions, and Br_orient_strArr is the magnetization.
StepHB_magnetPose	[a,b,n_mag,half_range] ;[r_mag,Br_orient_strArr]	The variables are the same as in the above.

5.4 Representative Outputs

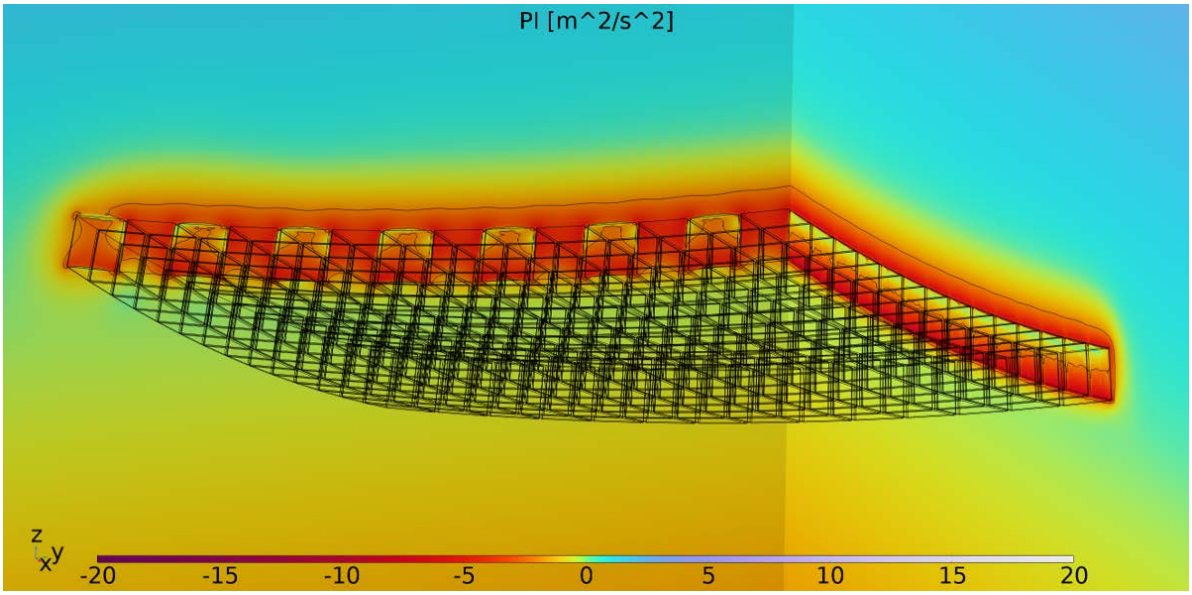

Fig. 9: 3D COMSOL simulation of the ferrofluid body force potential and equipotential lines at z = 11 mm.

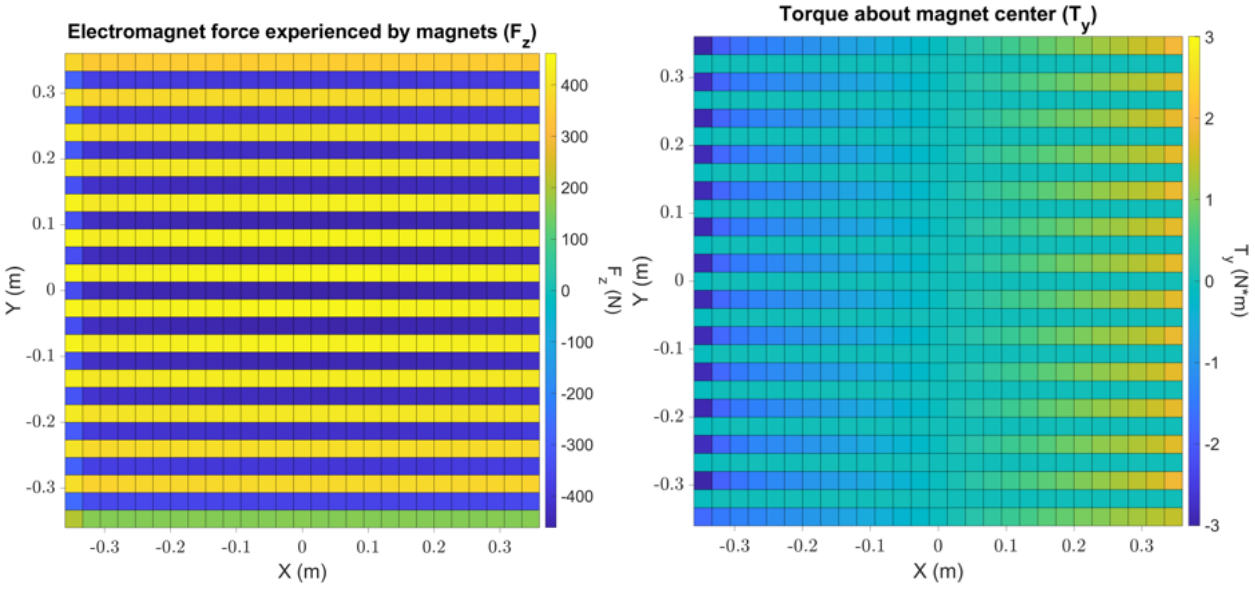

(a) z component of the force vectors

(b) y component of torque vectors

Fig. 10: Electromagnetic forces and torques induced by Halbach array on each individual magnet

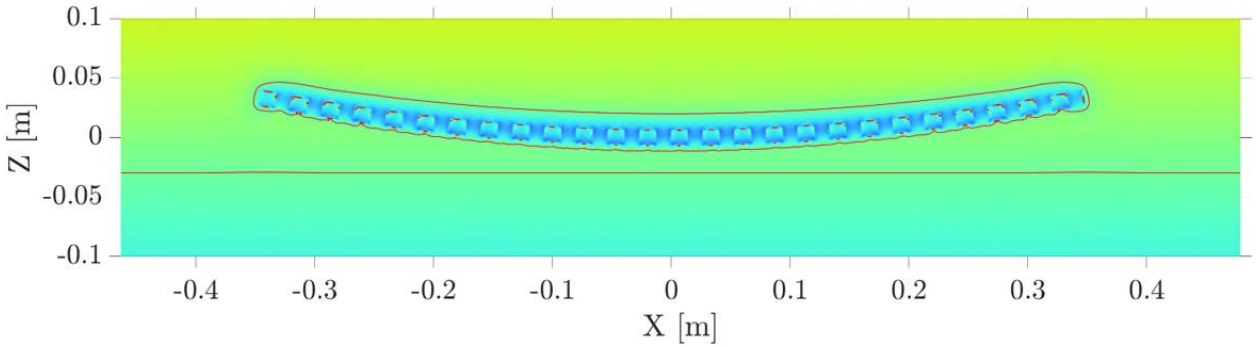

Fig. 11: Cutplane contour of body force potential, and the equipotential line evaluated at 2 cm above the origin

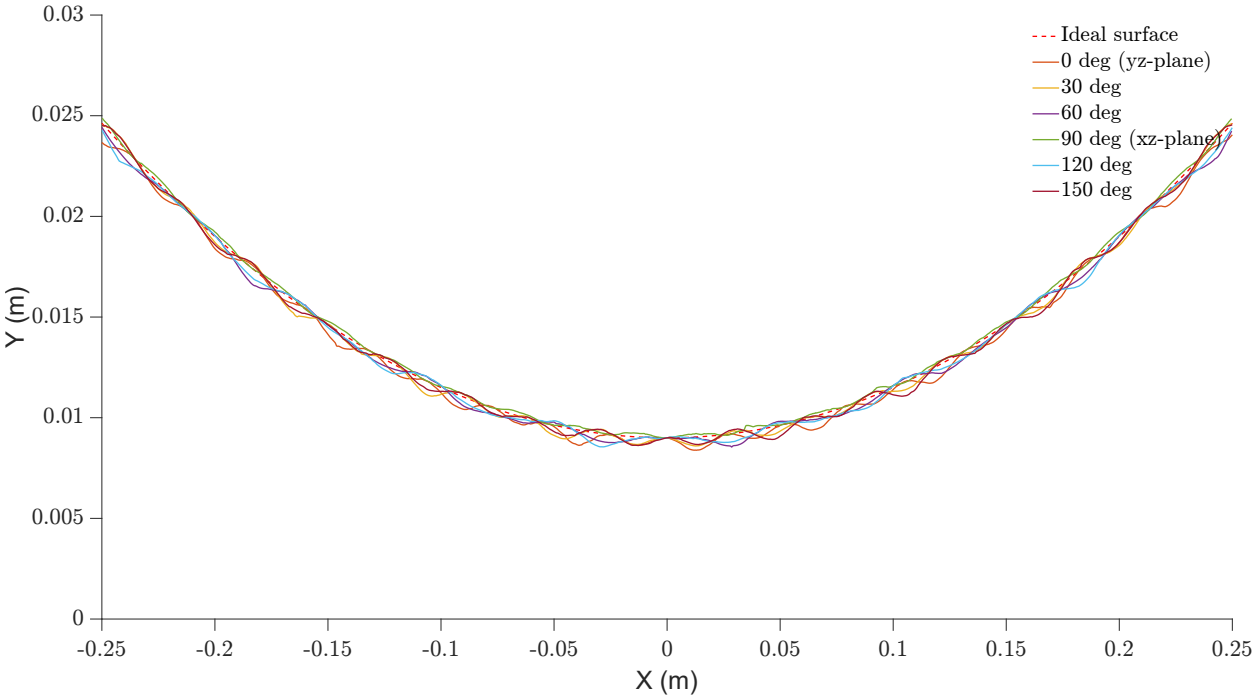

Fig. 12: Uncorrected equipotential lines in 6 cut planes and comparison with the ideal design surface of the ferrofluid

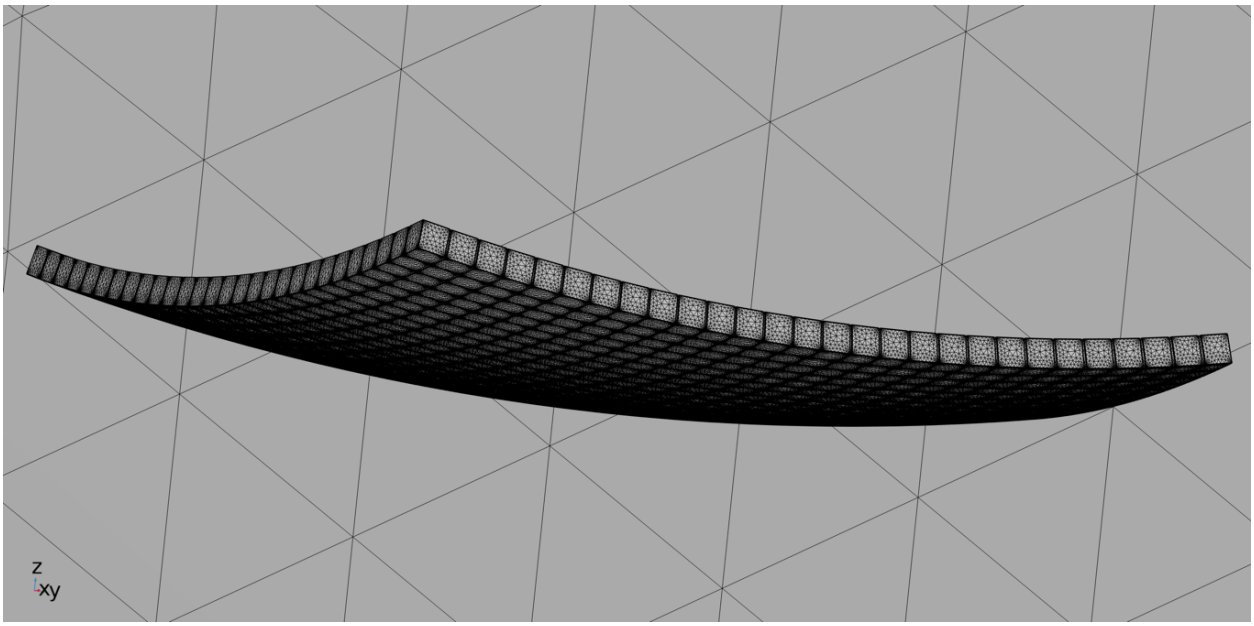

Fig. 13: Halbach array geometry

5.5 Simulation Parameters

Table 16: Descriptions for COMSOL parameters

Variable name	Description
w	Magnet width
d	Gap between magnets
n_mag	Number of magnets in one dimension
half_range	The last magnets location in half range of each dimension
a	Parabolic Halbach Array coefficients in x dimension
b	Parabolic Halbach Array coefficients in y dimension
h_ff2hb	Ferrofluid bottom to Halbach Array top distance[m]
h_pc2hb	Passive Corrector bottom to Halbach Array top distance [m]
delta_ff	Ferrofluid Thickness [m]
cutpoint	Position of cutpoint where to interpolate the body force potential
A	Passive Corrector Amplitude
eps	Passive Corrector minimum thickness
lambda_hb	Halbach array wavelength (4 magnets) [m]
lambda_pc_bottom	Passive Corrector bottom surface wavelength [m]
L_hb	Total Halbach Array length [m]
use_pc	Switch for adding a Passive Corrector
calculate_force	Switch for adding force calculation nodes for magnets
StepOrRotate	Switch for choosing Halbach Array allowing shift and rotation of magnets and Halbach Array only allowing shift of magnets
r_mag	The position of each magnet
k	single-rotation axis in cartesian coordinates of each magnet
psi	single-rotation angle [deg]

Br_orient_strArr	Remanent flux density orientation in material frame [deg]
f	waitbar handle
d_bottom	The function describing the flat passive corrector bottom surface
d_top	The function describing the flat passive corrector top surface
x_pc_bottom_min	Passive corrector bottom surface minimum in x dimension
x_pc_bottom_max	Passive corrector bottom surface maximum in x dimension
y_pc_bottom_min	Passive corrector bottom surface minimum in y dimension
y_pc_bottom_max	Passive corrector bottom surface maximum in y dimension
x_pc_top_min	Passive corrector top surface minimum in x dimension
x_pc_top_max	Passive corrector top surface maximum in x dimension
y_pc_top_min	Passive corrector top surface minimum in y dimension
y_pc_top_max	Passive corrector top surface maximum in y dimension
z_bottom	The function describing the z position of the Passive Corrector bottom surface
bottom_expression	Passive Corrector bottom surface expression used in COMSOL
z_top	The function describing the z position of the Passive Corrector top surface
top_expression	Passive Corrector top surface expression used in COMSOL
entity	A number sequence representing magnets used in COMSOL for assigning material, physics and mesh
Force_name	Force name buffer be used in global evaluation and plottings
Torque_name	Torque name buffer be used in global evaluation and plottings
PI_level	The ferrofluid body force potential evaluated at the cutpoint
Force_vector	A buffer storing the force data extracted from COMSOL model for plotting the 2D force map in MATLAB
Torque_vector	A buffer storing the torque data extracted from COMSOL model for plotting the 2D torque map in MATLAB
X	x coordinates of each magnets
Y	y coordinates of each magnets
Fx	Force in x direction
Fy	Force in y direction
Fz	Force in z direction
Tx	Torque in x direction
Ty	Torque in y direction
Tz	Torque in z direction
cb	colorbar handle
Fx_max	Maximum Force in x direction
Fx_min	Minimum Force in x direction
Fx_range	Range of Force in plotting
Fy_max	Maximum Force in y direction
Fy_min	Minimum Force in y direction
Fy_range	Range of Force in plotting
Fz_max	Maximum Force in z direction
Fz_min	Minimum Force in z direction
Fz_range	Range of Force in plotting
Tx_max	Maximum Torque in x direction
Tx_min	Minimum Torque in x direction

Tx_range	Range of Torque in plotting
Tx_max	Maximum Torque in y direction
Tx_min	Minimum Torque in y direction
Tx_range	Range of Torque in plotting
Tx_max	Maximum Torque in z direction
Tx_min	Minimum Torque in z direction
Tx_range	Range of Torque in plotting
Equipotential_surface	Switch for plotting equipotential surface
pd4	plotdata for plotgroup 4
pd5	plotdata for plotgroup 5
pd6	plotdata for plotgroup 6
pd7	plotdata for plotgroup 7
pd8	plotdata for plotgroup 8
pd9	plotdata for plotgroup 9
pd10	plotdata for plotgroup 10
x_ideal	Ideal surface x value
r_sphere	The radius of a sphere used for extracting data
focalLength	The focal length of the spherical surface
z_ideal	Ideal surface z value
ScanSphere_radius	The radius of a Scan sphere used to extract the data point
p_0deg	Data points from the 0 degree cut plane contour
p_30deg	Data points from the 30 degree cut plane contour
p_60deg	Data points from the 60 degree cut plane contour
p_90deg	Data points from the 90 degree cut plane contour
p_120deg	Data points from the 120 degree cut plane contour
p_150deg	Data points from the 150 degree cut plane contour
h_compensation	A height compensation used for making the equipotential lines aligned

6 Passive and Active Simulation

6.1 Purpose

The simulation procedure integrates both passive and active correctors using a coupled MATLAB and COMSOL approach. In this process, the geometry of the passive corrector, including parameters such as the dimensions of the Halbach array, is initially defined within MATLAB. These parameters are subsequently transferred to the COMSOL model, where the simulation is conducted. Additionally, variations in saturation magnetization can be specified as an input, enabling analysis of the system's behavior under different magnetic conditions.

Upon completion of the simulation, COMSOL sends the resulting data back to MATLAB for further processing. In MATLAB, the overall potential is evaluated to generate the EQP interface. Additionally, a Fast Fourier Transform (FFT) analysis is performed on this data. This seamless interaction between MATLAB and COMSOL is facilitated by COMSOL Livelink, which streamlines the design procedure and enables automation.

6.2 Assumptions

1. Magnetic and gravitational forces are considered.
2. The ferrofluid properties are interpolated from the data of existing FerroTec water-based ferrofluids.
3. The ferrofluid is assumed to follow the Langevin magnetization curve to calculate the body force potential.
4. The ferrofluidic surface is assumed to follow the equipotential profile after neglecting surface tension
5. A linear approximation of the B-H curve of the ferrofluid is adopted

6.3 Code Structure

Table 17: Code structure for Passive and Active Simulation

Section	Lines	Description	I/O
Introduction	1-14	Definition of code objectives	No
Code configuration	17-19	Clear variables, add paths to functions etc.	No
Passive-active correctors config.	21-24	Passive & Active correctors design parameters	Yes
Halbach parameters	27-35	Halbach array & magnet properties	Yes
Ferrofluid parameters	37-45	Ferrofluid properties	Yes
Constants	47-49	Physical constants used in the model	No
COMSOL file paths	51-53	COMSOL filename & paths	Yes
Halbach derived parameters	55-58	Additional experimental setup parameters	No
Store parameters	60-80	Storage of geometric parameters	No
Passive corrector geometry	82-90	Definition of passive corrector geometry	No
Store parameters	92-94	Storage of corrector parameters	No
Update COMSOL parameters	96-114	Update of COMSOL parameters from MATLAB	No
Update & rebuild geometry	117-121	Update & rebuild geometry in COMSOL	No
Material Selection	123-124	Reset material & physics in COMSOL	No
Run simulation	127	Run the COMSOL study	No
Extract data	130-141	Extract & interpolate data array from COMSOL	No

Convert data	144-146	Rearrange data extracted into suitable format	No
Evaluate Potential	149-152	Evaluate gravity & magnetic potential	No
Store parameters	155-163	Storage of simulation parameters	No
Define target profile	167-170	Define target deviation profile shape	No
Determine interface	173-178	Solve for the location of equipotential line	No
Calculate deviation	180-181	Calculate the deviation generated	No
Evaluate ideal corrector	185-187	Construct the perfect passive corrector	No
Plot interface	190-199	Plot equipotential interface & target profile	No
Calculate deviation	202-206	Calculate the maximum deviation from target	No
Store parameters	208-213	Storage of equipotential parameters	No
Fast Fourier Transformation	217-225	Conduct Fast Fourier Transformation (FFT)	No
Plot FFT	228-234	Plot the FFT results	No
Plot Formatting	238-246	Plot standardization	No
Calculate KBF	249-252	Calculate and store Kelvin Body Force (KBF)	No
Store data	256-258	Store plots and data	No

Table 18: Descriptions for functions used in Passive and Active Simulation

Function name	Description
createFit_RhoVsPhi	Creates a MATLAB curve fitting to the density and solute volume percentage data of the ferrofluid
createFit_PhiVsMs	Creates a MATLAB curve fitting to the solute volume percentage and saturation magnetization data of the ferrofluid
createFit_Chi0VsPhi	Creates a MATLAB curve fitting to the initial magnetic susceptibility and solute volume percentage data of the ferrofluid
get_Rho_Chi0_Phi	Interpolates the ferrofluid density, initial magnetic susceptibility, and solute volume percentage from saturation magnetization
magnetization	Calculates ferrofluid magnetization from the magnetic field
spacingconv	Convert and rearrange data accordingly for get_Rho_Chi0_Phi
Kelvin_B	Calculates the Kelvin Body force from magnetic flux density
gridinterp_Pi_m	Does a 3-dimensional interpolation of the magnetic potential
residuals_setPI	Determines the residual potential for the 3D equipotential interface

Table 19: I/O of functions used in Passive and Active Simulation

Function name	I/O	Comments
createFit_RhoVsPhi	[phi_data, rho_data] ;[fitresult, gof]	phi_data and rho_data are the ferrofluid solute volume percentage and density, respectively.
createFit_PhiVsMs	[Ms_data, phi_data] ;[fitresult, gof]	Ms_data and phi_data are the ferrofluid saturation magnetization and solute volume percentage, respectively.
createFit_Chi0VsPhi	[phi_data, Chi0_data] ;[fitresult, gof]	phi_data and Chi0_data are the ferrofluid solute volume percentage and initial magnetic susceptibility, respectively.

get_Rho_Chi0_Phi	[Ms] ;[rho,chi0,phi]	Ms,rho,chi0,and phi are the ferrofluid saturation magnetization, density, initial magnetic susceptibility, and solute volume percentage.
magnetization	[H,params];[M]	H is the magnetic field strength, params is the MATLAB structure containing general system parameters, and M is the ferrofluid magnetization.
spacingconv	[X,Y,x,y,f];[X,Y,F]	X & Y are the ferrofluid x & y coordinate array, x & y are the expanded X & Y arrays, f is the interpolated data from COMSOL X & Y are the inputs, F is the rearranged f.
Kelvin_B	[x,z,params];[Fk]	x is the simulation x coordinate, z is the simulation z coordinate params is the MATLAB structure containing general system parameters, and Fk is the Kelvin Body Force magnitude.
gridinterp_Pi_m	[x_m,z_m,H_m,params] ;[Pi_m]	x_m, z_m, and H_m are arrays corresponding to the horizontal and vertical positions, and the magnetic field strength over a grid. params is the MATLAB structure containing general system parameters, and Pi_m is an interpolant of the magnetic potential.
residuals_setPI	[Z, z0, params];[res]	Z is the vector of state (elevations of (x,y) points), z0 the target height at (0,0) params is the MATLAB structure containing general system parameters, and res is the vector of potential residuals

6.4 Representative Outputs

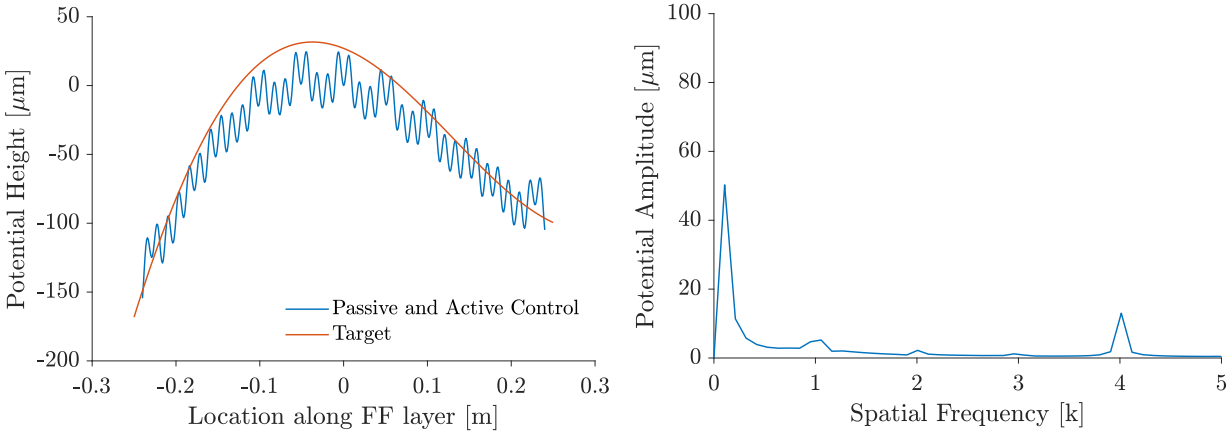

(a) Equipotential plot of the ferrofluid interface

(b) FFT analysis of the deviation

Fig. 14: Example equipotential plot and FFT analysis of the deviation under passive and active controls

7 Dependencies

7.1 Constitutive Equation

The constitutive equations are used to determine the properties of the ferrofluid through the interpolation of the Ferrotec EMG water-based ferrofluid series[1], given the saturation magnetization of the ferrofluid.

Table 20: Descriptions for the constitutive equation functions

Function name	Description
createFit_RhoVsPhi	Creates a MATLAB curve fitting to the density and solute volume percentage data of the ferrofluid
createFit_Chi0vsRho	Creates a MATLAB curve fitting to the initial magnetic susceptibility and density data of the ferrofluid
createFit_PhiVsMs	Creates a MATLAB curve fitting to the solute volume percentage and saturation magnetization data of the ferrofluid
createFit_Chi0VsPhi	Creates a MATLAB curve fitting to the initial magnetic susceptibility and solute volume percentage data of the ferrofluid
createFit_RhovsMs	Creates a MATLAB curve fitting to the density and saturation magnetization data of the ferrofluid
get_Rho_Chi0_Phi	Interpolates the ferrofluid density, initial magnetic susceptibility, and solute volume percentage from saturation magnetization

7.2 Magnetization

This function returns the magnetization vector module for a given external magnetic field.

Table 21: Code structure for magnetization

Section	Lines	Description
Introduction	2-14	Definition of code objectives
Parameters	17-18	Extracting parameters from params MATLAB structure
Calculating Magnetization vector	21-23	Calculating the magnetization from magnetic field assuming the Langevin curve

7.3 Magnetic Potential

The magnetic field of the Halbach array generates a magnetic potential on the ferrofluid, proportional to the integral of the magnetization. Assuming the ferrofluid follows a Langevin magnetization curve, this integral can be evaluated analytically in the magnetic potential code.

Table 22: Code structure for magnetic potential

Section	Lines	Description
Introduction	1-12	Definition of code objectives
Parameters	13-18	Extracting parameters from params MATLAB structure
Calculating Magnetic Field H	19-23	Calculating the magnetic H-field from the B-field, and evaluating the Langevin function integral
Calculate Mass Force Potential PI	24-26	Using the magnetic H-field and the Langevin function to calculate mass-specific potential

[1] https://ferrofluid.ferrotec.com/products/ferrofluid-emg/water/. Consulted on 05/04/2024

7.4 Kelvin Body Force

The Kelvin body force is the force generated by the ferrofluid in a magnetic field gradient. Since stronger magnetic fields generate higher potentials, a field gradient will generate a magnetic force on the ferrofluid in the direction of the steepest ascent. The Kelvin body force code simulates this from the magnetic flux density and its gradient. Two separate methods are used, either using the magnetic flux density B and the magnetic field H, yielding the same result.

Table 23: Code structure for Kelvin_B

Section	Lines	Description
Introduction	1-16	Definition of code objectives
Parameters	17-18	Extracting required parameters
Calculating Mass Force Potential	20-33	Calculating Mass Force Potential using magnetic flux density B

Table 24: Code structure for Kelvin_H

Section	Lines	Description
Introduction	1-15	Definition of code objectives
Parameters	18-21	Extracting required parameters
Calculating Mass Force Potential	24-28	Calculating Mass Force Potential using magnetic field H

REFERENCES

[1] K. Halbach, Applications of permanent magnets in accelerators and electron storage rings, Journal of Applied Physics 57 (1). doi:10.1063/1.335021.

[2] R. E. Rosensweig, Ferrohydrodynamics, Dover Publications, 1997.

[3] J. C. Mallinson, One-Sided Fluxes — A Magnetic Curiosity?, IEEE Trans. Magn. 9 (4) (1973) 678–682. doi:10.1109/TMAG.1973.1067714.

[4] A. Romero-Calvo, G. Cano-Gómez, H. Schaub, Diamagnetically enhanced electrolysis and phase separation in low gravity, AIAA Journal of Spacecraft and Rockets 59 (1) (2021) 1–13. doi:10.2514/1.A35021.

[5] A. Romero-Calvo, G. Cano-Gómez, T. H. Hermans, L. Parrilla Benítez, M. Herrada, E. Castro-Hernández, Total magnetic force on a ferrofluid droplet in microgravity, Experimental Thermal and Fluid Science 117 (2020) 110124. doi:10.1016/j.expthermflusci.2020.110124.

[6] A. Myshkis, V. Babskii, N. Kopachevskii, L. Slobozhanin, A. Tyuptsov, Low-gravity fluid mechanics: mathematical theory of capillary phenomena, Springer, 1987.

[7] J. D. Jackson, Classical electrodynamics, 3rd Edition, Wiley, New York, NY, 1999.

[8] J. L. Neuringer, R. E. Rosensweig, Ferrohydrodynamics, The Physics of Fluids 7 (12) (1964) 1927–1937.

[9] A. Romero-Calvo, M. Herrada, G. Cano-Gómez, H. Schaub, Fully coupled interface-tracking model for axisymmetric ferrohydrodynamic flows, Applied Mathematical Modelling 111 (2022) 836–861. doi:10.1016/j.apm.2022.06.046.

[10] N. Rowlands, A. Romero-Calvo, D. Stafford, R. Kamire, A. Childers, S. F. Yates, E. Rahislic, S. Zheng, P. Cameron, G. Cano-Gómez, H. Chen, T. Hu, E. Comstock, M. Herrada, Development of a self-assembling ferrofluidic ionic liquid mirror, in: SPIE Astronomical Telescopes + Instrumentation, Yokohama, JP, 2024.